



Science Arts & Métiers (SAM)

is an open access repository that collects the work of Arts et Métiers Institute of Technology researchers and makes it freely available over the web where possible.

This is an author-deposited version published in: <https://sam.ensam.eu>
Handle ID: <http://hdl.handle.net/10985/17328>

To cite this version :

Gnofam Jacques TCHEIN, Dimitri JACQUIN, Dominique COUPARD, Eric LACOSTE, Franck GIROT - Genesis of Microstructures in Friction Stir Welding of Ti-6Al-4V - Metallurgical and Materials Transactions A - Vol. 49, n°6, p.2113-2123 - 2018

Any correspondence concerning this service should be sent to the repository

Administrator : scienceouverte@ensam.eu



Genesis of microstructures in Friction Stir Welding of Ti-6Al-4V

Gnofam Jacques TCHEIN ^{a,c}, Dimitri JACQUIN ^a, Dominique COUPARD ^b, Eric LACOSTE ^a,
Franck GIROT MATA ^c

^a Univ. Bordeaux, I2M, CNRS, F-33400 Talence, France

^b Arts et Métiers ParisTech, I2M, CNRS, Esplanade Arts et Métiers, F-33400 Talence, France

^c University of the Basque Country, UPV/EHU, Faculty of Engineering, Department of Mechanical Engineering,
Alameda de Urquijo s/n, Bilbao, Bizkaia, Spain

Corresponding author:

Dimitri JACQUIN

I2M, UMR 5295, Site IUT - 15, rue Naudet - CS 10207 - 33175 - Gradignan Cedex – France

Tel.: (33)5 56 84 58 65 – Fax: (33)5 56 84 58 43 – email: dimitri.jacquin@u-bordeaux.fr

ABSTRACT

This paper is focused on the genesis of microstructures in Friction Stir Welding (FSW) of the Ti-6Al-4V alloy. Several titanium joints, initially prepared with 4 different pre-heat treatments, were processed by FSW. Detailed microstructural analyses were performed in order to investigate change in the microstructure during the process. In this work, the FSW processing allows a controlled and stable microstructure to be produced in the stirring zone, regardless of the initial heat treatment or the welding conditions. The welded material undergoes a severe thermo-mechanical treatment which can be divided into two steps. First, the friction in the shoulder and the plastic strain give rise to the necessary conditions to allow a continuous dynamic recrystallization (CDRX) of the β phase. This operation produces a fine and equiaxed β grain structure. Second, once the pin has moved away, the temperature decreases and the material undergoes a heat treatment equivalent to air quenching. The material thus exhibits a $\beta \rightarrow \beta + \alpha$ transformation with germination of a fine intergranular Widmanstätten phase within the ex-fully-recrystallized- β grains.

KEYWORDS

Friction Stir Welding, Ti-6Al-4V alloy, Microstructure, Heat treatment

I. INTRODUCTION

The Ti-6Al-4V alloy is widely used due to its good resistance to corrosion, high strength (even at high temperatures) and its biocompatibility. It has applications in several domains such as aeronautics, medical science and the automotive sector.

Due to titanium alloy's good mechanical properties, such as its high melting point and high hardness, mastering the shaping processes of titanium alloys remains a challenging task, especially as welding titanium by conventional methods usually leads to a decrease in its mechanical properties [1]. To overcome these problems, Friction Stir Welding (FSW) could be used to maintain enhanced mechanical properties.

Friction Stir Welding is a solid-state welding process. Its main advantage is that it avoids most of the solidification defects usually encountered with other welding methods. This is why it is mainly performed on low melting point alloys such as aluminium [2–7] and magnesium [8–10]. FSW on titanium alloys is still rarely studied because it requires much more expensive experimental resources such as a cooling system or expensive welding tools [11–14]. Experimental research on FSW can be classified into two categories: optimisation/control of the process and effects of different FSW parameters on the microstructure.

Concerning optimisation/control of Ti-6Al-4V FSW, Edwards and Ramulu [13] studied the influence of two process parameters: rotational speed and welding speed. They were able to find adequate rotational and welding speeds for different plate thicknesses. The welding parameters were found to influence microstructure, penetration, void formation, and tool wear. Shojaeefard et al. [15] worked on Friction Stir Welds of AA1100. Microstructural and mechanical properties were optimised by the Design Of Experiments method (DOE). The welding parameters were rotational speed, shoulder diameter and welding speed, while the properties to optimise were ultimate tensile strength, grain size, and hardness. They simulated grain size evolution and validated it by experimental results. They found that welding speed played a major role in affecting grain size, hardness, and ultimate tensile strength (UTS) of the weld. Currently, much work is focused on FSW studies of dissimilar alloys [4–6,16,17]. In these cases, the material in the welded zone consists of a mixture of the two base materials and the weld's mechanical properties are similar to those of the softer base material. Other studies are presently focused on tool wear mechanisms and tool materials used in FSW of Ti-6Al-4V [14,18,19]. W-Re, WC, p-CBN and W-La alloys are materials usually used for titanium alloys, but W-Re alloys are currently considered to be the most effective [14,20,21].

Regarding the effects of different FSW parameters on the material, Edwards and Ramulu [22] used thermocouples to determine the peak temperature in Ti-6Al-4V plates during FSW. By varying the welding and rotational speeds, temperatures were found to increase up to 1500K, leading to the conclusion that rotational speed has the dominant effect on the peak temperature and welding speed controls exposure time at peak temperatures. Zhang et al. [23] studied the microstructural and mechanical properties of Ti-6Al-4V weld joints for different welding and rotational speeds. They found that an increasing rotational speed led to decreasing hardnesses and tensile strengths. They observed a fully lamellar microstructure in the stirred zone and a duplex structure in the heat affected zone. Yoon et al. [24] studied the effect of tool rotational speed on microstructure and texture evolution during FSW of equiaxed Ti-6Al-4V plates. Inside the Stirred Zone a fully lamellar structure was observed near the top surface, while a fully equiaxed structure was found near the bottom surface of the weld. Esmaily et al. [25] studied the mechanisms of formation of the martensitic phase in Ti-6Al-4V FS welds. They welded several samples at different rotational speeds and constant welding speeds. They pointed out that a minimum rotational speed is necessary to obtain the martensitic phase in the stirred zone. Using this value, they obtained a bimodal structure.

The Ti-6Al-4V alloy is one of the most commonly used titanium alloy grades, and its mechanical properties can be easily modified by heat treatment. In this paper, we propose to study the influence of different pre-heat treatments on the genesis of microstructures in FSW of the Ti-6Al-4V alloy.

II. EXPERIMENTAL PROCEDURES

A. Heat treatments

Before welding, 5 mm thick commercial purity Ti-6Al-4V plates were heat treated. The chemical composition of this alloy is presented in Table 1. Table 2 shows the different pre-heat treatments performed before welding. Three of the most common heat treatments [26,27] were applied under argon shielding gas. These heat treatments result in a change in microstructure and mechanical properties (Figure 1).

The microstructure of the initial (without pre-heat treatment) material comes from a relatively complex thermo-mechanical treatment in the $\alpha+\beta$ two-phase domain of the Ti-6Al-4V alloy. This treatment is used to break some of the α_p (primary) laths already formed. The α_p is formed during the solution heat-treatment in the $\alpha+\beta$ domain. During the rolling of the sheets, α_p debris can coalesce and recrystallize into small nodules which grow to become nodular primary α grains (α_{pn}). The size of these grains depends on the temperature and the duration of

the heat treatment. These nodules can only be completely re-dissolved if the material is heated above β -transus temperature (995°C). The β_m and β_s phases are trapped outside the nodules to form a β matrix. The metastable β_m phase corresponds to the non-equilibrium primary β phase, capable of being transformed and which can be maintained at ambient temperature by a local chemical composition which remains close to that of high temperatures. The stable β_s phase at room temperature is the primary β phase maintained at ambient temperature and stable due to a local concentration of β -stabiliser sufficient to maintain it, e.g. 15% of vanadium [28].

Both Figure 1.b and Figure 1.c show a primary lamellar α -phase called the Widmanstätten phase. The shape of the laths depends on the duration of the heat treatments and the cooling rates: the slower the cooling, the larger the laths.

Figure 1.b (coarse lamellar) shows an intergranular Widmanstätten α -phase (α_{WI}) surrounded by β and grain boundary Widmanstätten α -phase (α_{WGB}). The latter germinates at the prior β -grain boundaries in a particular orientation with the β phase (Burgers relations). It grows towards the inside of the grain in the form of laths. The germination and growth of this phase is accompanied by a diffusion of (a) α -stabiliser elements towards the laths, and (b) β -stabilisers outside these laths.

Figure 1.c (fine lamellar) shows only an intergranular Widmanstätten α -phase surrounded by β . This phase germinates inside the ex- β grains on sites such as dislocations or other defects. It is in the form of laths, either parallel (forming colonies of the same orientation), or entangled with two or three privileged orientations in the whole grain. These directions are often disoriented at 60°, corresponding to the angle between the 6 transformation variants from β to α . In this structure, intragranular α is surrounded by β_m or β_s depending on the stability of the matrix.

Finally, an annealing heat treatment at the top of the $\alpha + \beta$ domain was performed (Figure 1.d). This treatment stabilises the microstructure by dissolving the fine laths of α . The α -stabiliser alloying elements of this phase diffuse during the heat treatment and allow the growth of the nodular primary α grains (α_{pn}). During cooling, the β_m phase is transformed into β transformed (β_t) grains and the intergranular α -laths formed grow to varying degrees, depending on the cooling rate. This microstructure is called the duplex phase, and consists of equiaxed alpha grains (light) in a transformed beta matrix (dark) containing a coarse, acicular α phase.

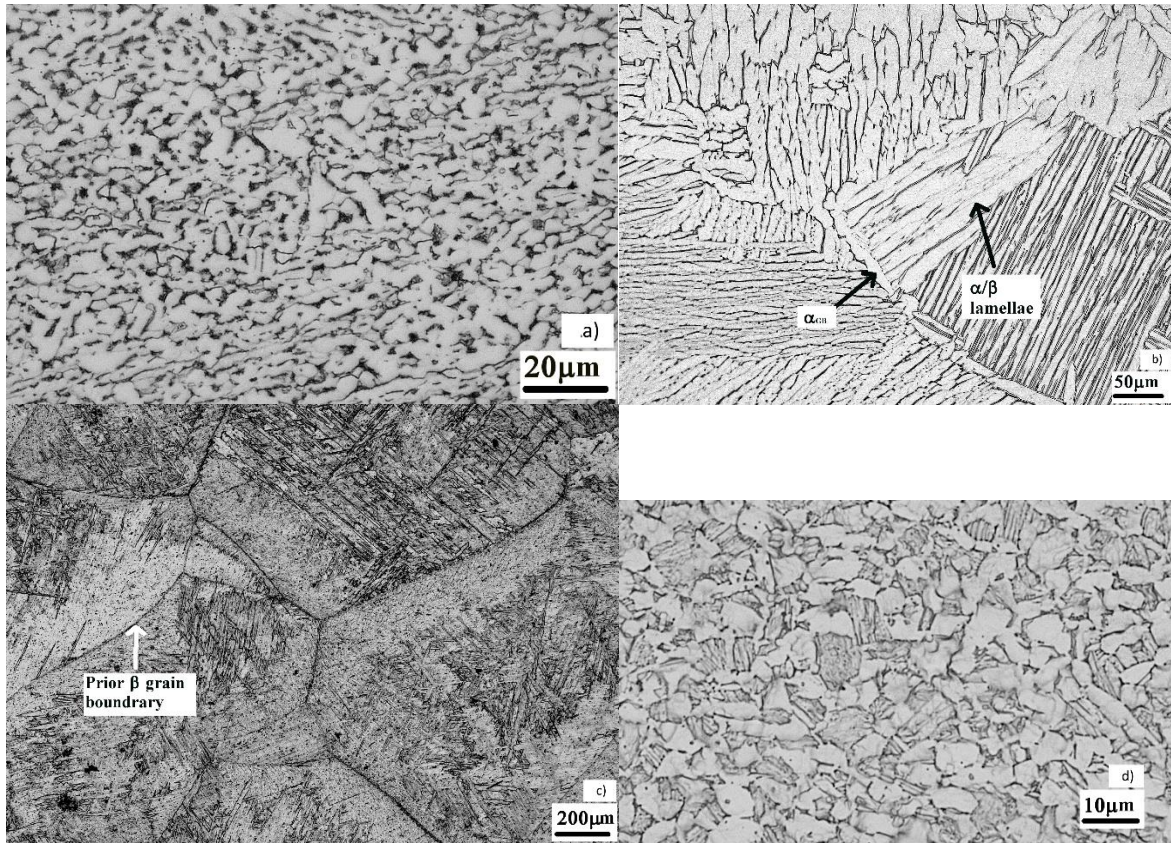


Figure 1 - Optical micrographs of different microstructures obtained by pre-heat treatments (a) initial material, (b) coarse lamellar, (c) fine lamellar, (d) duplex.

B. FSW process

FSW joints were created at LORTEK Research Centre (Ordizia, Spain) using MTS ISTIR PDS FSW equipment in position control with (1) a tilt angle of 2.5° and (2) a position control strategy. The spindle of the welding machine was connected to a cooling system, in order to reduce its temperature by a water flow. A 20 l/min argon gas flow was also used to prevent oxidation of the welds. A W-25Re welding tool with a convex shoulder and conical pin was chosen (Figure 2). The shoulder diameter and the pin length were 12 mm and 2.8 mm respectively. 3 mm penetration was made in full matter for 120 mm transversally to the rolling direction of the plates. The plates were clamped to a stainless-steel backing plate. Calibration tests were initially performed to choose the optimal sets of parameters giving sound welds. During those tests, the experimental windows was limited to Welding Speed encompassed between 50 and 95 mm/min and Rotational Speed encompassed between 400 rpm and 460 rpm, outside of this window the weld were defective: we observe flash, tunnel defects, or no stir.

Numerous experiments were carried out, by varying the initial pre-heat treatment, of course, but also the welding speed and the rotational speed, to be sure that each initial pre-heat treatment would at least produce a defect-free weld. Table 3 summarises all the experiments carried out.

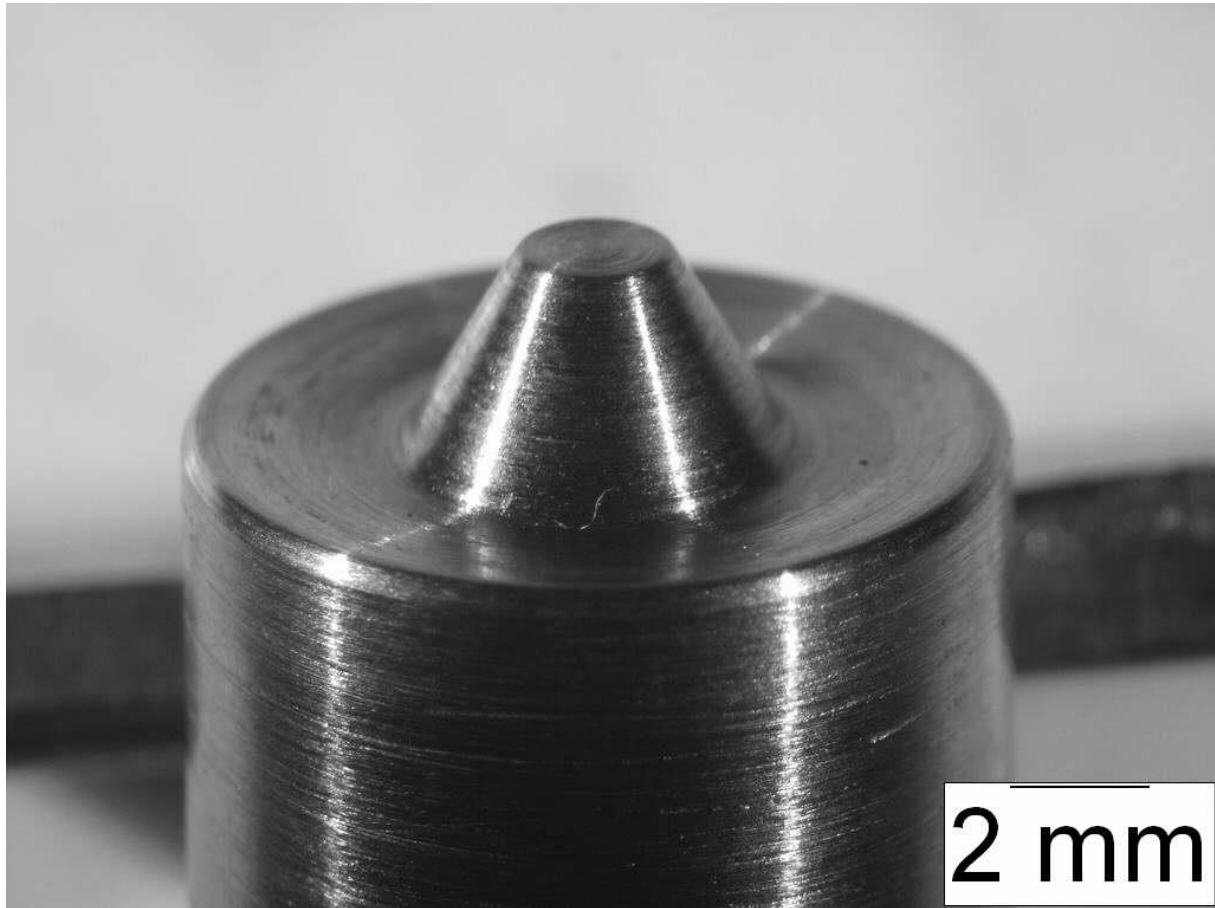


Figure 2 - W-25Re welding tool.

C. Design of experiments (DOE)

In order to study the effect of welding and rotational speed of the tool, a design of experiments was set up. Table 3 shows the L16 Taguchi table used for the experiments.

The results of the DOE were hardness along the weld and optical micrographs of the welds. Vickers hardness tests across the welds were carried out in a transversal section across all the zones (BM, TAZ, SZ, TAZ, and BM), 1 mm below the top surface of each weld. The testing conditions used were a load of 5 kg and a dwelling time of 10 s. The samples for microstructural observations were prepared by polishing with SiC abrasive papers. The polishing procedure started from very coarse P180 papers (200 μm SiC particle diameter) to P4000 (5 μm SiC particle diameter). The final polishing was done with colloidal silica. Finally, the specimens were etched

with Kroll's reagent (2 ml HF + 5 ml HNO₃ + 100 ml H₂O) for light optical microscope (OM) observations, or underwent electrolytic polishing (600 mL CH₃OH + 360 mL C₆H₁₄O₂ + 60 mL HClO₄, 30V, 5-10 s) for EBSD analysis.

III. RESULTS AND DISCUSSION

A. Microstructural analysis

The microstructural characterisation of sample no. 5 (coarse lamellar, speed 50 mm/min, rotation 420 rpm) is presented in Figure 3. One can clearly see that this FSW joint has no macroscopic defects such as porosity, lack of penetration, etc.

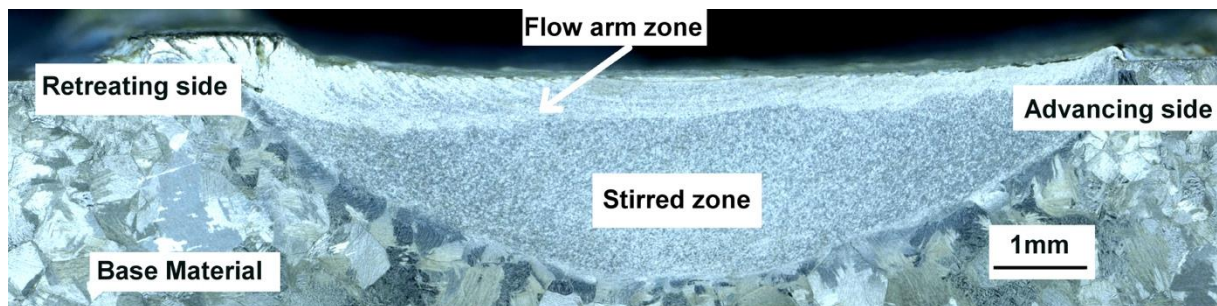


Figure 3 - Cross-section perpendicular to the welding direction of a coarse lamellar sample welded at 50 mm/min*420 rpm.

This sample shows a typical morphology for titanium alloy FSW joints. The base metal (BM), which is located far from the welded zone, undergoes no deformation or overheating. It therefore retains its original properties and microstructure. The heat affected zone (HAZ) undergoes heating without significant strain. The granular texture is identical to that of the base metal, but the dislocation population and the state of precipitation can change.

The thermo-mechanically affected zone (TMAZ) experiences both heating and plastic deformation during FSW, being characterised by a deformed structure brought about by the mechanical stirring of the tool. In the case of the present work, the TMAZ is limited to a very thin layer, due to the low thermal conductivity of titanium alloys and given that the pin is not threaded. The stirred zone (SZ), or nugget, undergoes the greatest plastic strain and temperature rise. The SZ is slightly larger than the pin.

Figure 4 shows the optical micrographs of the welding joints obtained with the four different initial microstructures. Each processing condition shows a similar microstructure in the SZ, which means that the changes occurring during the welding process are driven by the process itself. The initial heat-treatments have no significant effect on the microstructure of the welding zone.

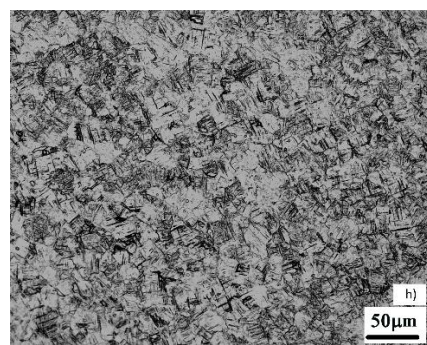
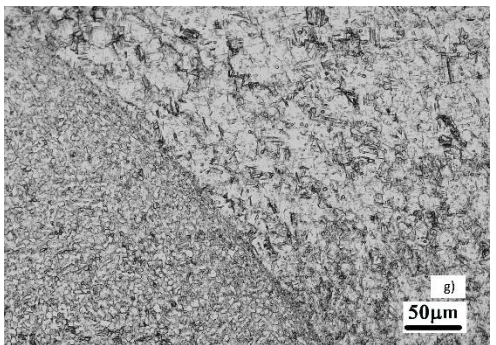
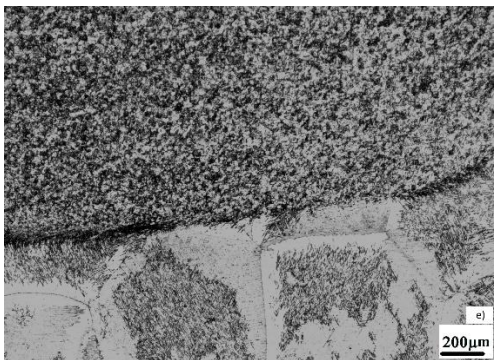
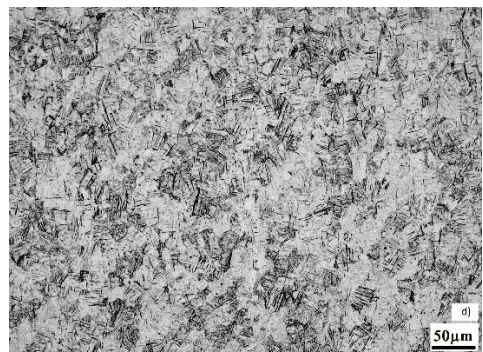
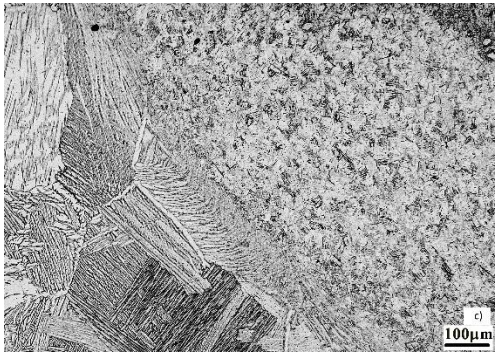
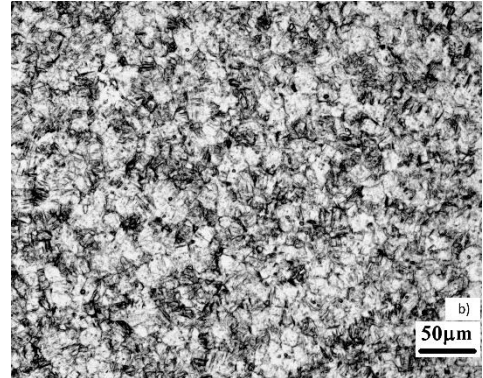
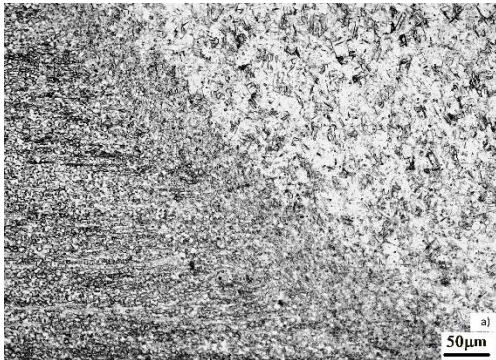


Figure 4 - Optical micrographs: a) Initial microstructure: boundaries between SZ and BM (65 mm/min and 420 rpm), b) Initial microstructure: SZ (65 mm/min and 420 rpm), c) Coarse lamellar: boundaries between SZ and BM (50 mm/min and 420 rpm), d) Coarse lamellar: SZ (50 mm/min and 420 rpm), e) Fine lamellar: boundaries between SZ and BM (50 mm/min and 440 rpm), f) Fine lamellar: SZ (50 mm/min and 440 rpm), g) Duplex: boundaries between SZ and BM (50 mm/min and 460 rpm), h) Duplex: SZ (50 mm/min and 460 rpm).

Figure 5 shows a typical backscattered SEM image obtained in the SZ. Equiaxed cells composed of a fine intergranular Widmanstätten phase can be observed. The size of the cells (around 13-14 μm) is nearly the same, whatever the initial microstructure and welding conditions. The FSW processing produces a grain size reduction in the SZ for the large grains (grain size reduces from 735 μm and 573 μm to 13-14 μm , for β annealed pre-treated samples), or an increase in grain size for the initial small grains (grain size increases from 6.5 μm to 13-14 μm for untreated and $\alpha+\beta$ annealed pre-treated samples).

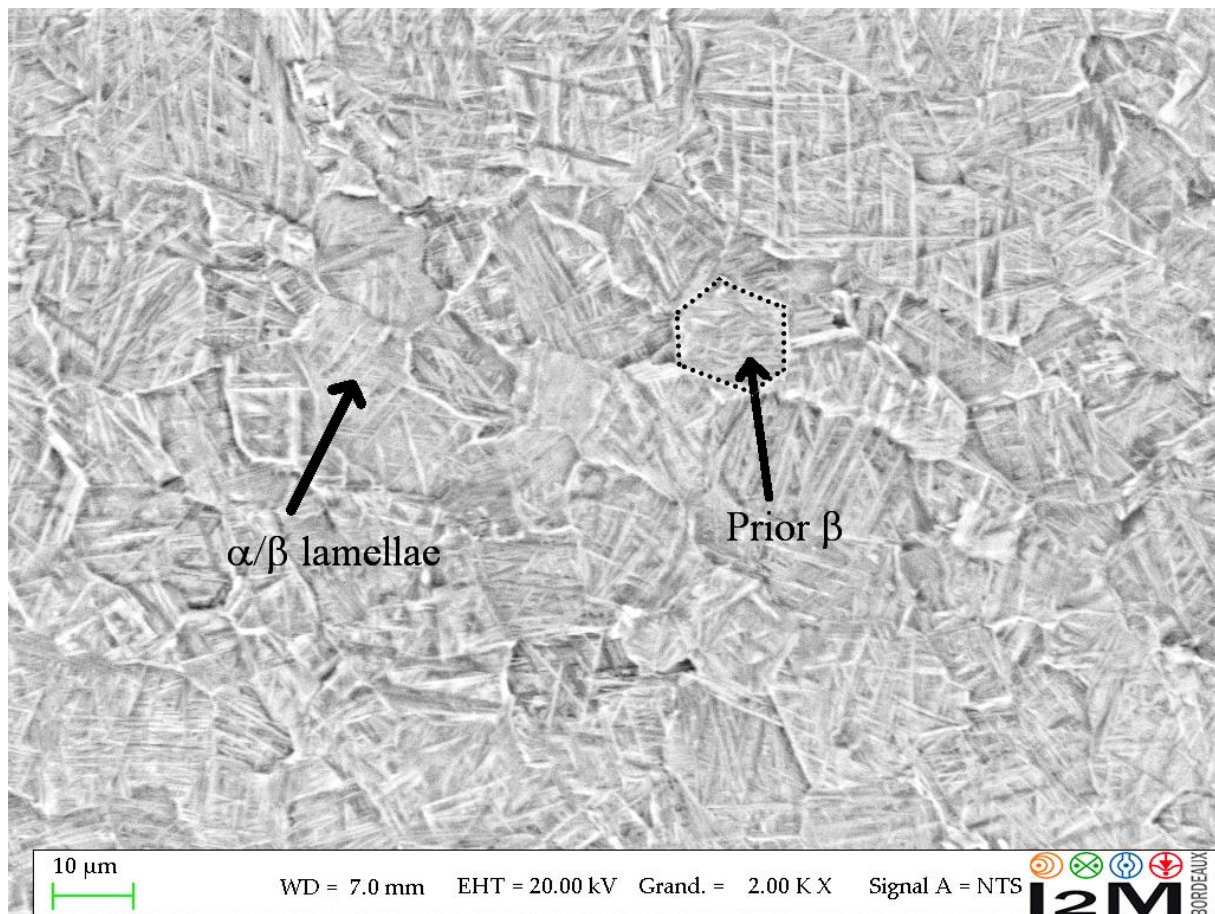


Figure 5 - Backscattered SEM image in the SZ of the fine lamellar sample welded at 50 mm/min and 440 rpm.

The fine intergranular Widmanstätten phase in the SZ is characterised by a fully β transformed structure (α/β lamellar structures). This suggests that (a) the peak temperatures in the SZ exceeded the β transus temperature during the process [29], and (b) the $\beta \rightarrow \alpha + \beta$ phase transformation occurred during cooling for all types of welds, regardless of the initial heat treatment or process parameters.

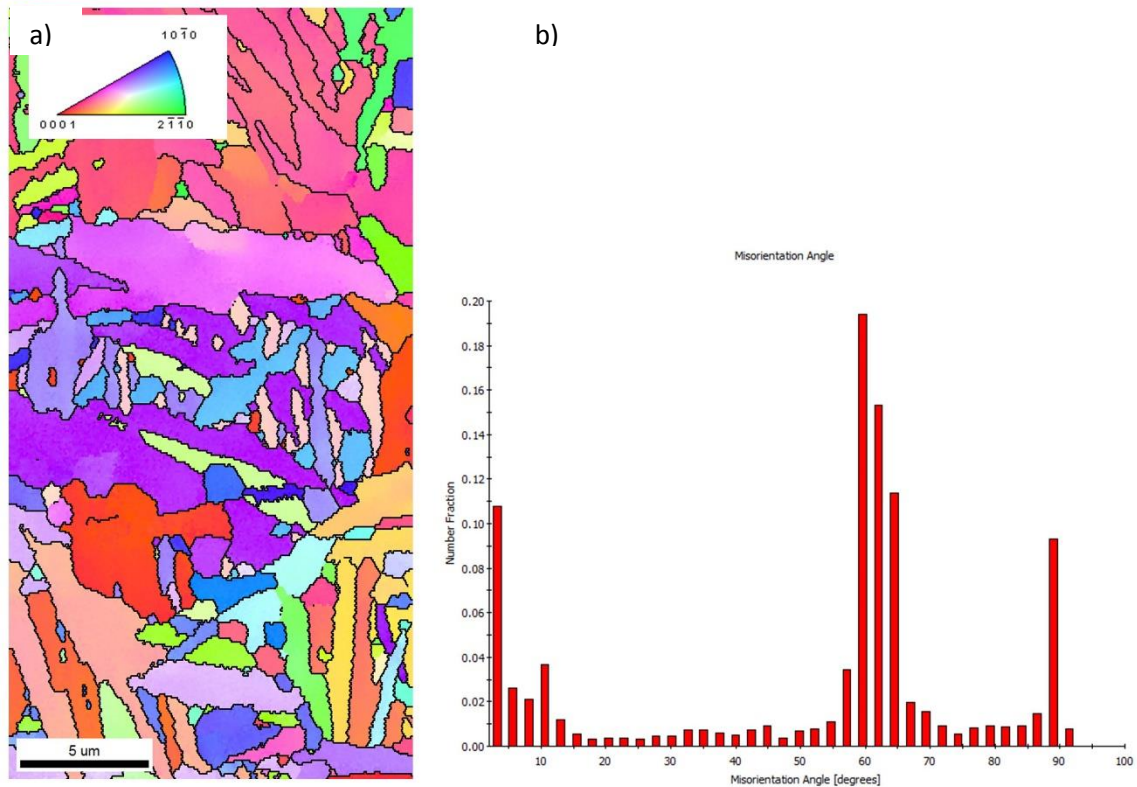


Figure 6 - OIM images of α phase in the ZS of the fine equiaxed sample welded at 50 mm/min and 400 rpm: (a) inverse pole figure map, (b) statistical misorientation angle distribution

Figure 6 shows the microstructure obtained by the EBSD technique coupled with OIM equipment. An OIM scan was performed in the SZ centre for sample no. 1 (Table 3). The resolution of the SEM was too low to identify the very fine β phase, but the good indexation of the hexagonal close-packed α phase revealed a typical basket-weave microstructure occurring during the $\beta \rightarrow \alpha + \beta$ transformation. This indicates that the structure is not strain-hardened, which shows that this transformation occurs after the plastic deformation, that is to say during the cooling phase. The very thin alpha laths suggest that the cooling rate is quite high, similar to air quenching. The misorientation distribution of the α grains shows a significant peak for the misorientation of 60° , which confirms

the $\beta \rightarrow \alpha + \beta$ transformation, given that transformed α and β phases satisfy the Burgers orientation relationship defined by $(110)_\beta // (0001)_\alpha$, $[\bar{1}\bar{1}\bar{1}]_\beta // [2\bar{1}\bar{1}0]_\alpha$ and $(\bar{1}12)_\beta // (01\bar{1}0)_\alpha$ [30,31].

B. Genesis of microstructures

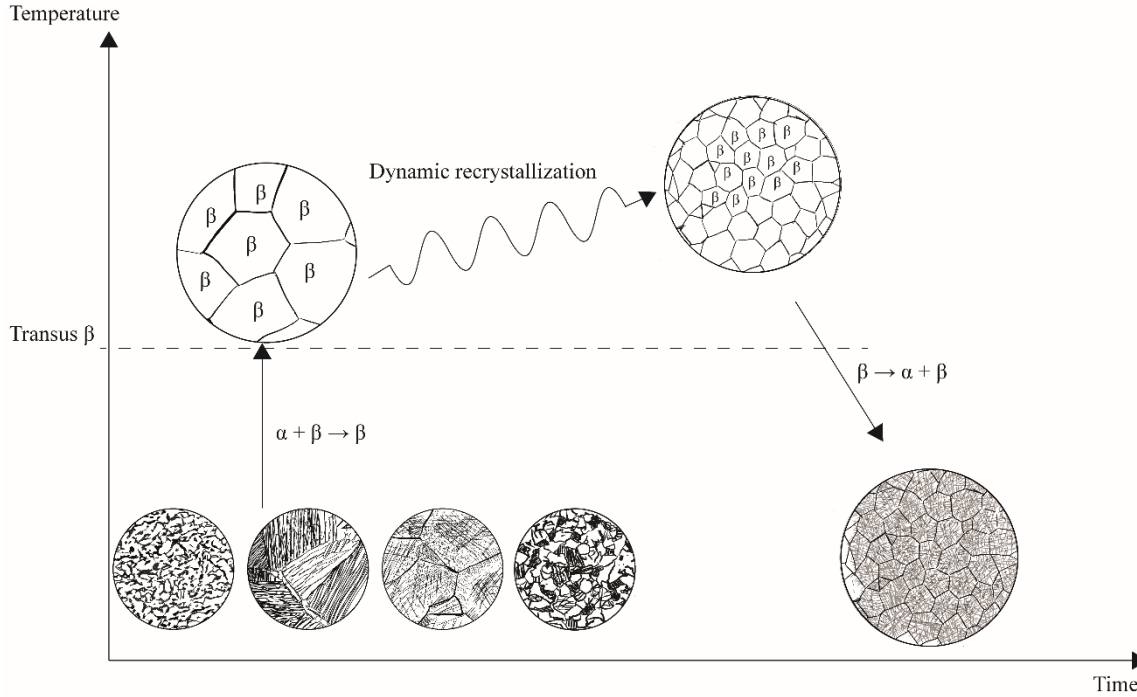


Figure 7 - Thermomechanical steps followed by the material during the FSW process

Figure 7 shows the various thermomechanical steps followed by the material during the welding process.

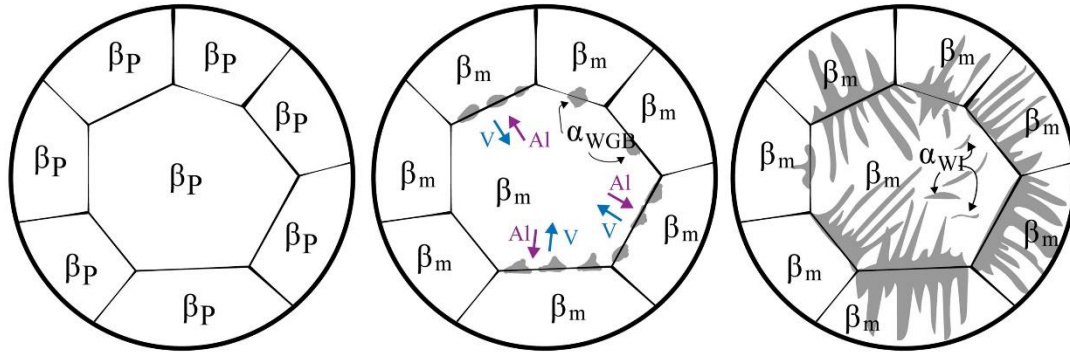
First, the material undergoes a sudden rise in temperature, caused by (a) friction between the tool shoulder and pin, and (b) plastic deformation. The resulting high temperature coupled with the plastic deformation tends to promote a condition of dynamic recrystallization [32–34], which takes place usually at temperatures between 0.6 and 0.8 times the melting temperature T_m . For Ti-6Al-4V, T_m is about 1933 K, so that the DRX starting temperature is about 1160 K, which is below the β transus (1268 K). Montheillet et al. [35] showed that the “classical discontinuous” dynamic recrystallization occurring by nucleation and growth of the new grains is not observed in the β phase of the titanium alloy (due to the high rate of dynamic recovery associated with the large stacking fault energy of the bcc structure). Instead, continuous dynamic recrystallization (CDRX) takes place, i.e., grain fragmentation occurs by the generation of new grain boundaries [36]. This mechanism generates reduced and equiaxed grains that could be much smaller than the initial one. R. Ding and al. [37] investigated

dynamic and/or metadynamic recrystallization when the Ti-6Al-4V alloy was processed in the β -phase field. The author obtained a similar recrystallized grain with embedded martensitic phase, as in Figure 6. In this paper, the recrystallized grain size stabilises at around 13-14 μm , regardless of the initial heat treatment or process parameters, which suggests that the CDRX mechanism predominates with respect to β grain growth. It is known that β grain growth is rapid in the β phase field because of high temperatures and the absence of second-phase particles to impede grain boundary motion, but this phenomenon is totally masked in our case by the recrystallization phenomenon.

Afterwards, when the pin has moved away, heating by friction and by plastic power decreases drastically. Considering the low thermal conductivity of the Ti-6Al-4V alloy, it can be supposed that the material undergoes air quenching from the β phase field. In this case, during the rapid cooling, the β phase that is stable at high temperature will transform (at least partially) into a very fine intergranular lath phase. This transformation is similar to one occurring during the germination of an intergranular Widmanstätten phase (the same as one used for the fine lamellar heat treatment).

The α phase precipitates preferentially at the prior β grain boundary. Colonies of α_{WGB} lamellae then develop from this precipitation. Simultaneously, for fast cooling rates, a new α_1 phase develops in the matrix, forming sub-colonies. (Figure 8). The difference between the diffusion coefficients of the α -stabiliser and β -stabiliser elements imposes growth of the platelet-shaped α phase.

The air quenching undergone by the material is between 25 and 45°C/s approximately [38], but this is not enough to produce the α' martensitic phase, which requires a cooling rate of $> 160^\circ\text{C/s}$ [39].



β_P : β prior

β_m : β metastable

α_{WGB} : α grain boundary

α_{WI} : α intergranular

Figure 8 - $\beta \rightarrow \beta + \alpha$ Widmanstätten phase transformation

C. Vickers hardness profile

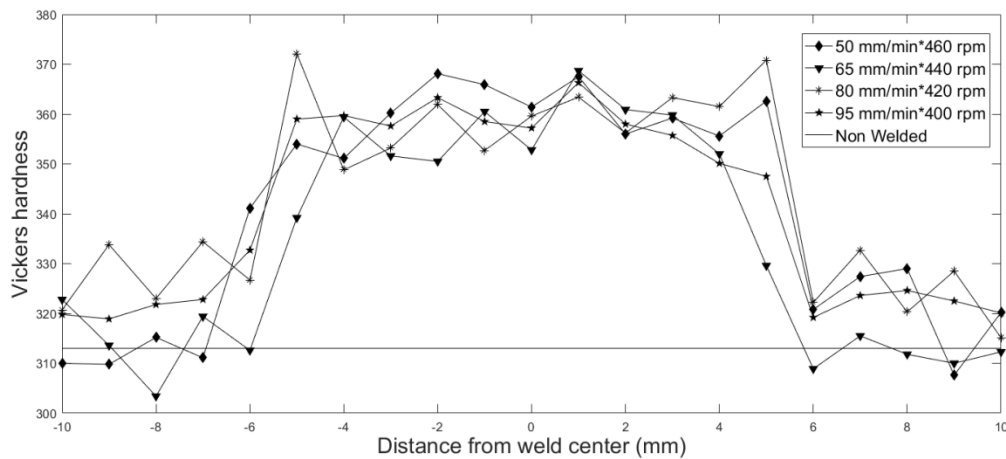


Figure 9 - Vickers Hardness profile across the weld for duplex base materials

Typical Vickers hardness profiles across the welds are shown in Figure 9. The higher Vickers hardness is observed in the stirred zone. The hardness in the base material is similar to that measured in non-welded samples. It is commonly accepted that conventional physicochemical hardening (quenching) does not produce

any significant hardening for titanium and its alloys. The increase in hardness in the stirred zone can be explained by the microstructure refinement in that zone according to the Hall-Petch relationship,

$$H = H_0 + k_h \cdot d^{1/2}$$

where H is the hardness, H_0 and K_h , two constants, and d, the grain size. The thin transition of hardness between the SZ and the BM indicates that the HAZ is very thin, if not almost non-existent. The mean hardness in the SZ (Table 3) is calculated by averaging the hardness of the nine central values around the centreline of the weld. According to Table 3, the mean hardness is not sensitive to the welding process parameters, given the very small difference (7.85 HV) between the highest and lowest values. According to other reports on FSW of Ti-6Al-4V [23], this is due to the narrow window for rotational speed and welding speed values.

A simplified analysis of the variance was performed to give a clear picture of how far the process parameter affects the response and the level of significance of the factor considered. The results of the Design of experiments and the calculated response table for hardness are shown in Table 4 and Table 5 respectively. From the main effects plotted in Figure 10, the optimal parametric combination for hardness optimisation is A3B4C2. The ANOVA table for means is calculated and listed in Table 6. The F test is being carried out to study the significance of the process parameters. The high F value indicates that the factor is highly significant in affecting the response of the process. The ANOVA table for hardness shows that initial microstructure may have the maximum effect on hardness while welding speed and rotation have less effect. Nevertheless, the response table for hardness shows a very low variation for initial microstructure, proving that hardness in the stirred zone is not sensitive to pre-heat treatment.

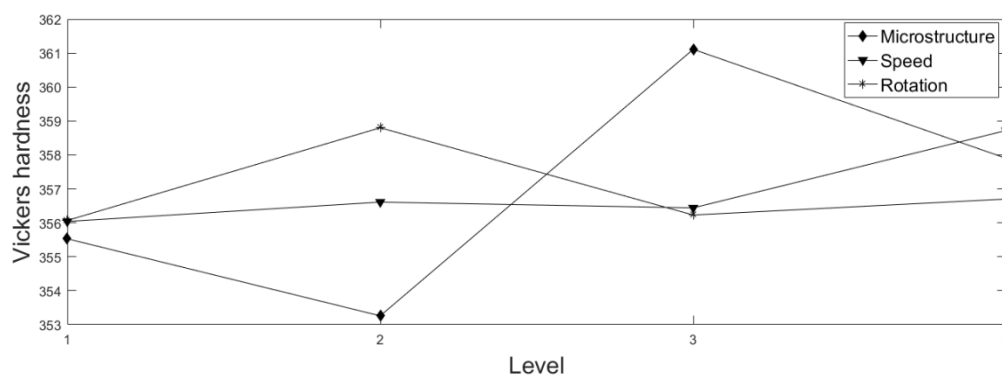


Figure 10: Main Effects plot for Hardness

IV. CONCLUSION

Several titanium joints, initially prepared with 4 different pre-heat treatments, were processed in FSW. Detailed microstructural analyses were performed in order to investigate the change in microstructure occurring during the process.

The main conclusions drawn from this study are as follows:

- 1) The FSW of Ti-6Al-4V produces a very thin TMAZ.
- 2) During Friction Stir Welding of the Ti-6Al-4V alloy, the maximum temperature increase exceeds the β -transus temperature.
- 3) The FSW processing produces a controlled and stable microstructure in the stirring zone, whatever the initial heat treatment or the welding conditions. This microstructure is characterised by a fully β -transformed structure in the form of lamellar α/β structures, resulting from the $\beta \rightarrow \alpha + \beta$ phase transformation. A typical basket-weave microstructure can be observed, with a 60° predominant misorientation. The thin α laths are grouped within cells corresponding to the ex- β grains present before the air quenching.
- 4) The genesis of the microstructure can be divided into two steps. First, the plastic strain and the friction allow a sufficient temperature to be reached and plastic strain to achieve a continuous dynamic recrystallization (CRDX), which produces a stable β grain size of around 13-14 μm . A reduction in grain size can be seen for large grains, corresponding to an initial heat-treatment above the β transus, and an increase in grain size can be seen for the initial small grains. Second, a fine $\beta \rightarrow \beta + \alpha$ Widmanstätten phase transformation appears within the *ex-fully-recrystallized*- β grains.
- 5) Hardness in the stirred zone is not sensitive to pre-heat treatment.

Acknowledgements

This work was supported by IdEx Bordeaux within the framework of the Cross-border Joint Laboratory “Aquitania Euskadi Network In Green Manufacturing and Ecodesign” (LTC AENIGME). The authors gratefully

322 acknowledge Egoitz Aldemando (Ik4- LORTEK Research Centre, Ordizia, Spain) for carrying out the FSW
323 joining.

324

325 REFERENCES

- 326 1. V.S. Godiganur, S. Biradar: *Int. J. Res. Eng. Technol.*, 2014, vol. 3, pp. 572–576.
- 327 2. C. He, Y. Liu, J. Dong, Q. Wang, D. Wagner, C. Bathias: *Int. J. Fatigue*, 2015, vol. 81, pp. 171–178.
- 328 3. P. Cavaliere, A. Squillace, F. Panella: *J. Mater. Process. Technol.*, 2008, vol. 200, pp. 364–372.
- 329 4. M.M.Z. Ahmed, S. Ataya, M.M. El-Sayed Seleman, H.R. Ammar: *J. Mater. Process. Technol.*, 2017, vol.
330 242, pp. 77–91.
- 331 5. S.R. Kumar, V.S. Rao, R.V. Pranesh: *Procedia Mater. Sci.*, 2014, vol. 5, pp. 1726–1735.
- 332 6. M. Koilraj, V. Sundareswaran, S. Vijayan, S.R. Koteswara Rao: *Mater. Des.*, 2012, vol. 42, pp. 1–7.
- 333 7. A.H. Lotfi, S. Nourouzi: *Metall. Mater. Trans. A.*, 2014, vol. 45, pp. 2792–2807.
- 334 8. Y.S. Sato, S.H.C. Park, A. Matsunaga, A. Honda, H. Kokawa: *J. Mater. Sci.*, 2005, vol. 40, pp. 637–642.
- 335 9. J. Chen, R. Ueji, H. Fujii: *Mater. Des.*, 2015, vol. 76, pp. 181–189.
- 336 10. S.H.C. Park, Y.S. Sato, H. Kokawa: *Scr. Mater.*, 2003, vol. 49, pp. 161–166.
- 337 11. Y. Zhang, Y.S. Sato, H. Kokawa, S.H.C. Park: *Mater. Sci. Eng. A.*, 2008, vol. 488, pp. 25–30.
- 338 12. H. Fujii, Y. Sun, H. Kato, K. Nakata: *Mater. Sci. Eng. A.*, 2010, vol. 527, pp. 3386–3391.
- 339 13. P. Edwards, M. Ramulu: *J. Eng. Mater. Technol.*, 2010, vol. 132, 031006 (10 pages).
- 340 14. Y.N. Zhang, X. Cao, S. Larose, P. Wanjara: *Can. Metall. Q.*, 2012, vol. 51, pp. 250–261.
- 341 15. M.H. Shojaeefard, M. Akbari, A. Khalkhali, P. Asadi, A.H. Parivar: *Mater. Des.*, 2014, vol. 64, pp. 660–666.
- 342 16. Ş. Kasman: *Int. J. Adv. Manuf. Technol.*, 2013, vol. 68, pp. 795–804.
- 343 17. N.M. Daniolos, D.I. Pantelis: *Int. J. Adv. Manuf. Technol.*, 2017, vol. 88, pp. 2497–2505.
- 344 18. J. Wang, J. Su, R.S. Mishra, R. Xu, J.A. Baumann: *Wear.*, 2014, vol. 321, pp. 25–32.
- 345 19. A. Farias, G.F. Batalha, E.F. Prados, R. Magnabosco: *Wear.*, 2013, vol. 302, pp. 1327–1333.
- 346 20. L. Zhou, H.J. Liu, P. Liu, Q.W. Liu: *Scripta Mat.*, 2009, vol. 61, pp. 596–599.
- 347 21. H.J. Liu, L. Zhou, Q.W. Liu: *Mater. Des.*, 2010, vol. 31, pp. 1650–1655.
- 348 22. P. Edwards, M. Ramulu: *Sci. Technol. Weld. Join.*, 2010, vol. 15, pp. 468–472.
- 349 23. Y. Zhang, Y.S. Sato, H. Kokawa, S.H.C. Park, S. Hirano: *Mater. Sci. Eng. A.*, 2008, vol. 485, pp. 448–455.
- 350 24. S. Yoon, R. Ueji, H. Fujii: *Mater. Charact.*, 2015, vol. 106, pp. 352–358.
- 351 25. M. Esmaily, S. Nooshin Mortazavi, P. Todehfarah, M. Rashidi: *Mater. Des.*, 2013, vol. 47, pp. 143–150.
- 352 26. Y. Combres, C. Champin: *Tech. Ing.*, 1995, M1335. 33, pp. 24.

353 27. ASM International, ed., *Metallography and microstructures*, New ed, American Society for Metals, Metals
354 Park, Ohio, 2004.

355 28. B. Hocheid, R. Klima, C. Beauvais, M. Rapin, C. Roux: *Mém Sci Rev Mét.*, 1970, vol. 72, pp. 583–590.

356 29. J. Su, J. Wang, R.S. Mishra, R. Xu, J.A. Baumann: *Mater. Sci. Eng. A.*, 2013, vol. 573, pp. 67–74.

357 30. M. Humbert, L. Germain, N. Gey, E. Boucard: *Acta Mater.*, 2015, vol. 82, pp. 137–144.

358 31. S.C. Wang, M. Aindow, M.J. Starink: *Acta Mater.*, 2003, vol. 51, pp. 2485–2503.

359 32. E. Ghasemi, A. Zarei-Hanzaki, E. Farabi, K. Tesař, A. Jäger, M. Rezaee: *J. Alloys Compd.*, 2017, vol. 695,
360 pp. 1706–1718.

361 33. X.G. Fan, H. Yang, P.F. Gao, R. Zuo, P.H. Lei: *J. Mater. Process. Technol.*, 2016, vol. 234, pp. 290–299.

362 34. S. Lu, D. Ouyang, X. Cui, K. Wang: *Trans. Nonferrous Met. Soc. China.*, 2016, vol. 26, pp. 1003–1010.

363 35. F. Montheillet, L. Pallot, D. Piot: *7th Int. Conf. on Processing and Manufacturing of Advanced Materials,*
364 *THERMEC 2011*, vol. 706-709, Quebec City, QC, 2012.

365 36. S. Gourdet, F. Montheillet: *Acta Mater.*, 2003, vol. 51, pp. 2685–2699.

366 37. R. Ding, Z.X. Guo, A. Wilson: *Mater. Sci. Eng. A.*, 2002, vol. 327, pp. 233–245.

367 38. A. Bardelcik, C.P. Salisbury, S. Winkler, M.A. Wells, M.J. Worswick: *Lightweight Struct.*, 2010, vol. 37, pp.
368 694–702.

369 39. F. Le Maitre: *Revue de Métallurgie*, 1970, vol.67, pp. 563.

FIGURE CAPTIONS

Figure 1 - Optical micrographs of different microstructures obtained by pre-heat treatments (a) initial material, (b) coarse lamellar, (c) fine lamellar, (d) duplex

Figure 2 - W-25Re welding tool

Figure 3 - Cross-section perpendicular to the welding direction of a coarse lamellar sample welded at 50 mm/min*420 rpm.

Figure 4 - Optical micrographs

(a) Initial microstructure: boundaries between SZ and BM (65 mm/min and 420 rpm)

(b) Initial microstructure: SZ (65 mm/min and 420 rpm)

(c) Coarse lamellar: boundaries between SZ and BM (50 mm/min and 420 rpm)

(d) Coarse lamellar: SZ (50 mm/min and 420 rpm)

(e) Fine lamellar: boundaries between SZ and BM (50 mm/min and 440 rpm)

(f) Fine lamellar: SZ (50 mm/min and 440 rpm)

(g) Duplex: boundaries between SZ and BM (50 mm/min and 460 rpm)

(h) Duplex: SZ (50 mm/min and 460 rpm)

Figure 5 - Backscattered SEM image in the SZ of the fine lamellar sample welded at 50 mm/min and 440 rpm

Figure 6 - OIM images of α phase in the ZS of the fine equiaxed sample welded at 50 mm/min and 400 rpm: (a) inverse pole figure map, (b) statistical misorientation angle distribution

Figure 7 - Thermomechanical steps followed by the material during the FSW process

Figure 8 - $\beta \rightarrow \beta + \alpha$ Widmanstätten phase transformation

Figure 9 - Vickers Hardness profile across the weld for duplex base materials